Supplementary Information for

Surface hydrogen migration significantly promotes electroreduction of acetonitrile to ethylamine

Yulong Tang,[1#] Jiejie Li,[1,2#] Yichao Lin,[1,2*] Moxing Cheng,[1] Shuibo Wang,[1,2] Ziqi Tian,[1,2*] Junjie Zhou,[1,2] Haolei, Zhang,[1] Yunan, Wang,[1,2] Liang Chen[1,2*]

[1] Zhejiang Key Laboratory of Advanced Fuel Cells and Electrolyzers Technology, Ningbo Institute of Materials Technology and Engineering, Chinese Academy of Sciences, Ningbo, Zhejiang 315201, P.R. China

[2] University of Chinese Academy of Sciences, Beijing 100049, P.R. China

Table of Contents

1. Supplementary Figures

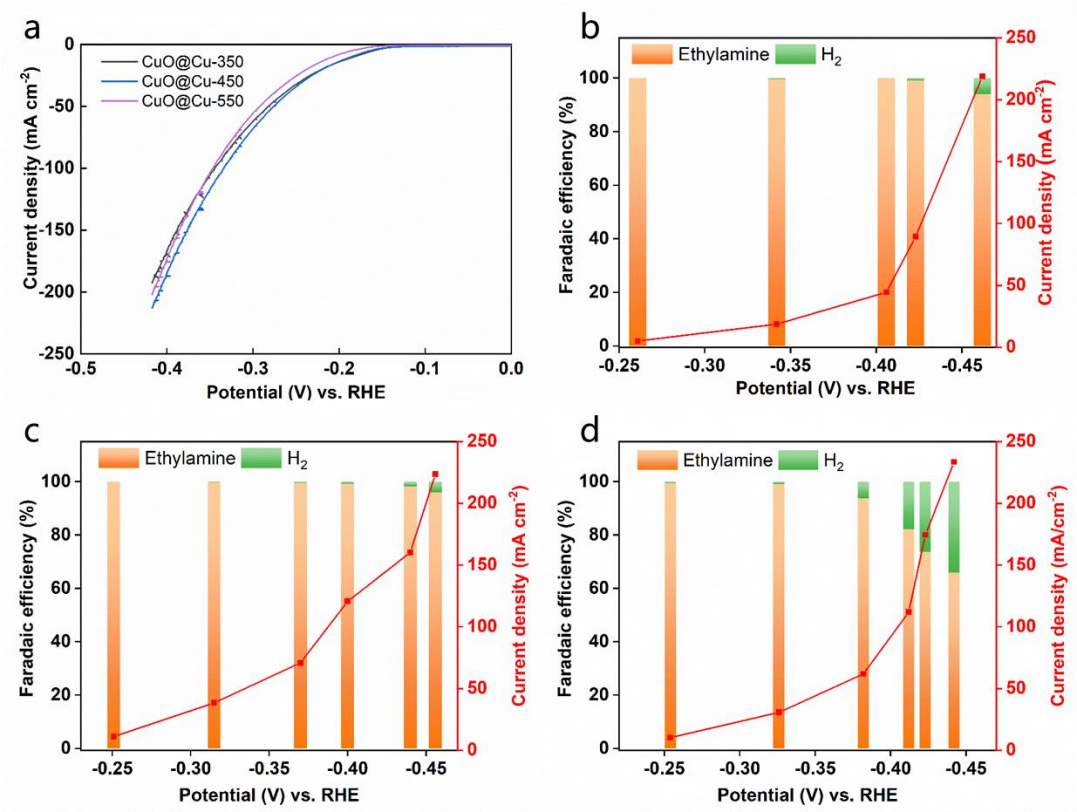

Supplementary Fig. 1 | Electrochemical measurements for CuO@Cu annealed at different temperatures. (a) LSV curves of CuO@Cu-T; (b) FE_{EA} at different potentials in CuO@Cu-350; (c) FE_{EA} at different potentials in CuO@Cu-450; (d) FE_{EA} at different potentials in CuO@Cu-550. The potentials in Fig. 1a-d are provided after 100% iR correction. Source data for Supplementary Fig. 1 are provided as a Source Data file.

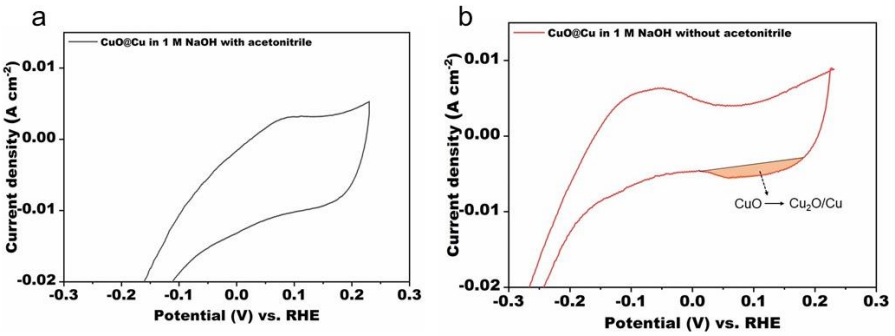

Supplementary Fig. 2 | CV curves of CuO@Cu heterostructure. (a) The CV curve of CuO@Cu heterostructure in 1.0 M NaOH with acetonitrile; (b) The CV curve of CuO@Cu heterostructure in 1.0 M NaOH without acetonitrile. The potentials in Supplementary Fig. 2a-b are provided after 100% iR correction. Source data for Supplementary Fig. 2 are provided as a Source Data file.

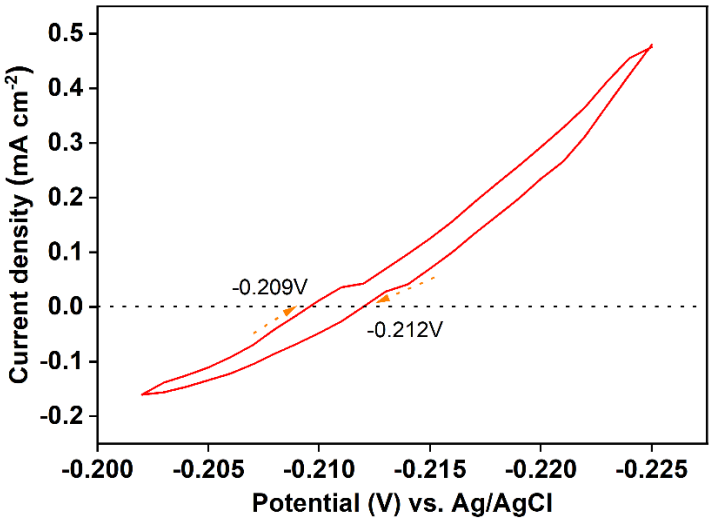

Supplementary Fig. 3 | Calibration test for Ag/AgCl reference electrode. The Ag/AgCl reference electrode was calibrated in a 0.5 M H_2SO_4 solution saturated with hydrogen by monitoring hydrogen oxidation and evolution reactions at a platinum wire electrode. The potential at which the current was zero was defined as 0 V relative to the reversible hydrogen electrode (RHE). The potentials in Supplementary Fig. 3 are provided without iR correction. Source data for Supplementary Fig. 3 are provided as a Source Data file.

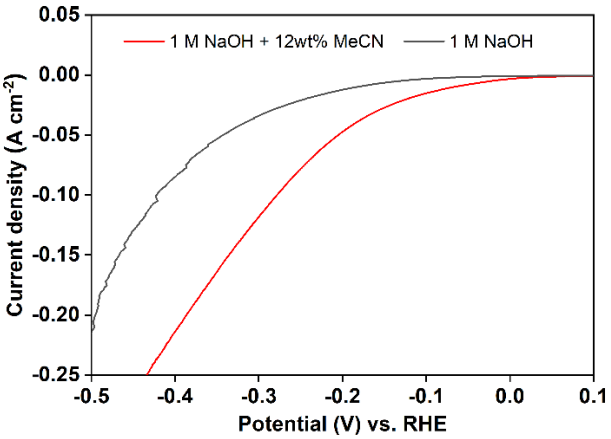

Supplementary Fig. 4 | LSV curves of CuO@Cu heterostructure in 1 M NaOH solution with and without acetonitrile. The potentials in Supplementary Fig. 4 are provided after 100% iR correction. Source data for Supplementary Fig. 4 are provided as a Source Data file.

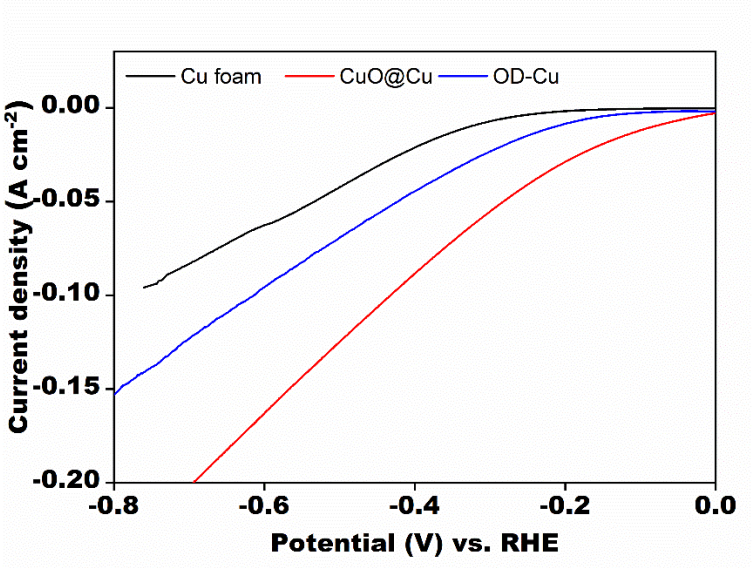

Supplementary Fig. 5 | LSV plots of CuO@Cu, OD-Cu and Cu foam in 1M NaOH containing 12 wt% acetonitrile without iR compensation. Source data for Supplementary Fig. 5 are provided as a Source Data file.

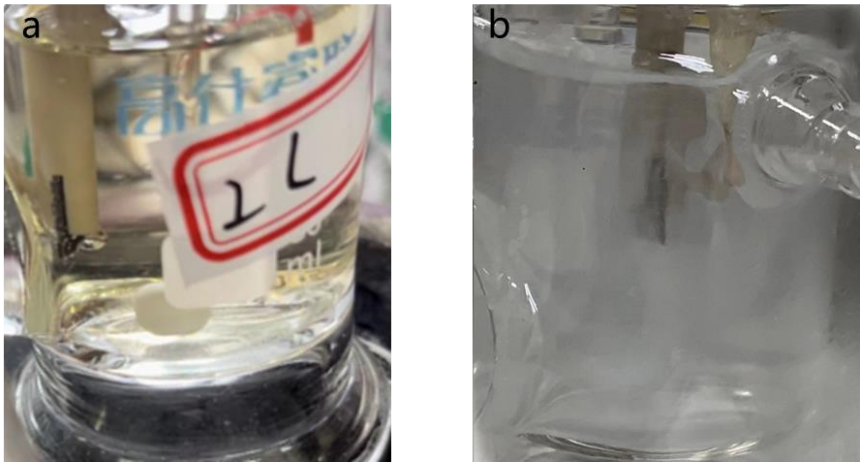

Supplementary Fig. 6 | Photos of the cathode in H-type cell under ARR test. (a) CuO@Cu; (b) Cu/CF-350.

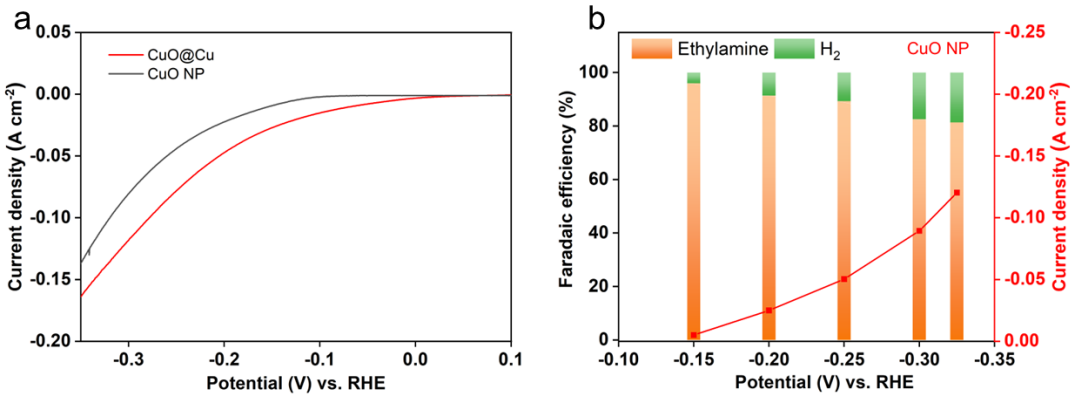

Supplementary Fig. 7 | Electrochemical measurements. (a) LSV curves of CuO@Cu and CuO NP in 1 M NaOH solution with acetonitrile; (b) FE_{EA} at different potentials for CuO NP. The potentials in Supplementary Fig. 7a-b are provided after 100% iR correction Source data for Supplementary Fig. 7 are provided as a Source Data file.

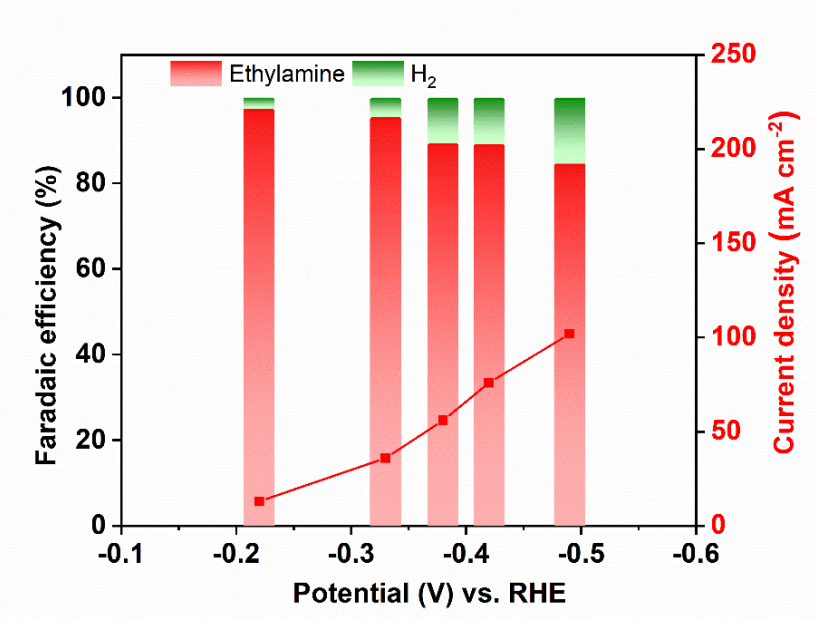

Supplementary Fig. 8 | FE_{EA} of OD-Cu at different potentials. The potentials in Supplementary Fig. 8 are provided after 100% iR correction. Source data for Supplementary Fig. 8 are provided as a Source Data file.

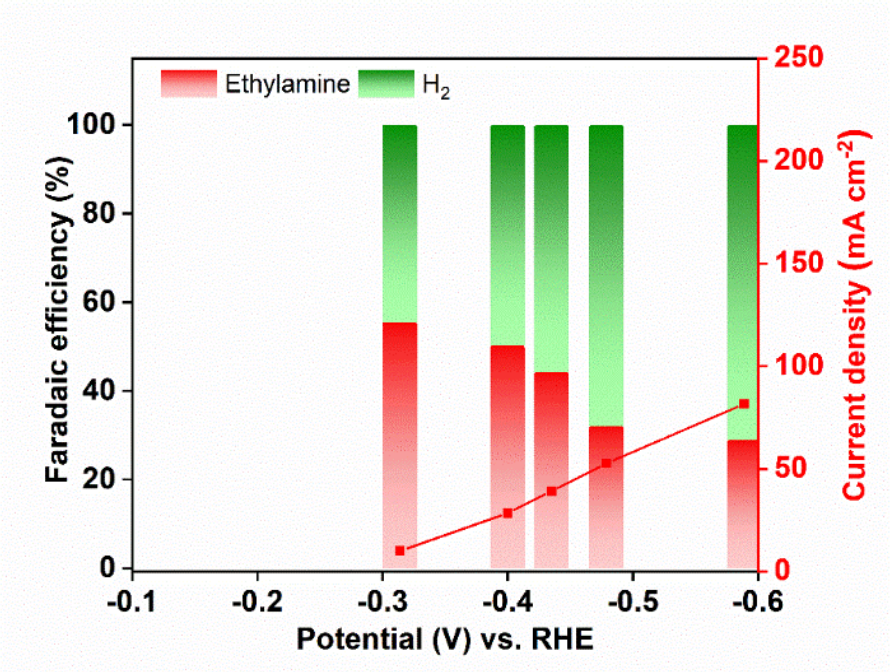

Supplementary Fig. 9 | FE_{EA} at different potentials in Cu foam. The potentials in Supplementary Fig. 9 are provided after 100% iR correction. Source data for Supplementary Fig. 9 are provided as a Source Data file.

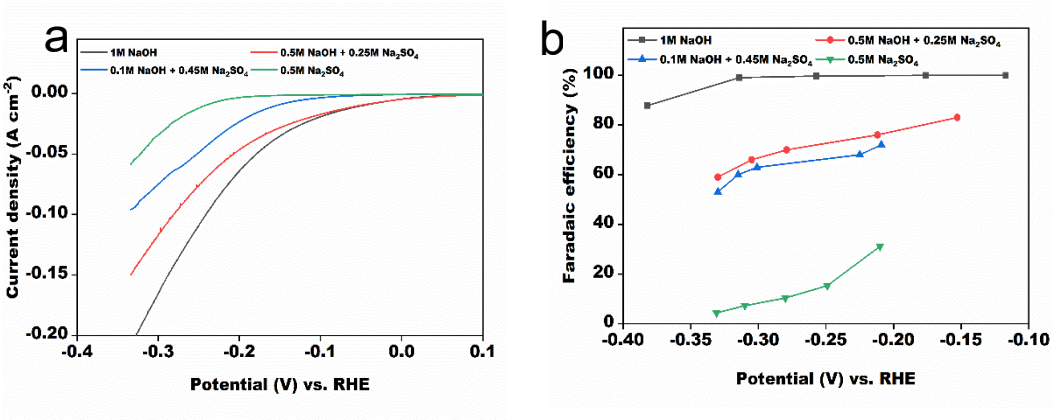

Supplementary Fig. 10 |Electrochemical measurements. (a) LSV curves of CuO@Cu in different electrolyte; (b) the corresponding FE_{EA} at different potentials. The potentials in Supplementary Fig. 10a-b are provided after 100% iR correction. Source data for Supplementary Fig. 10 are provided as a Source Data file.

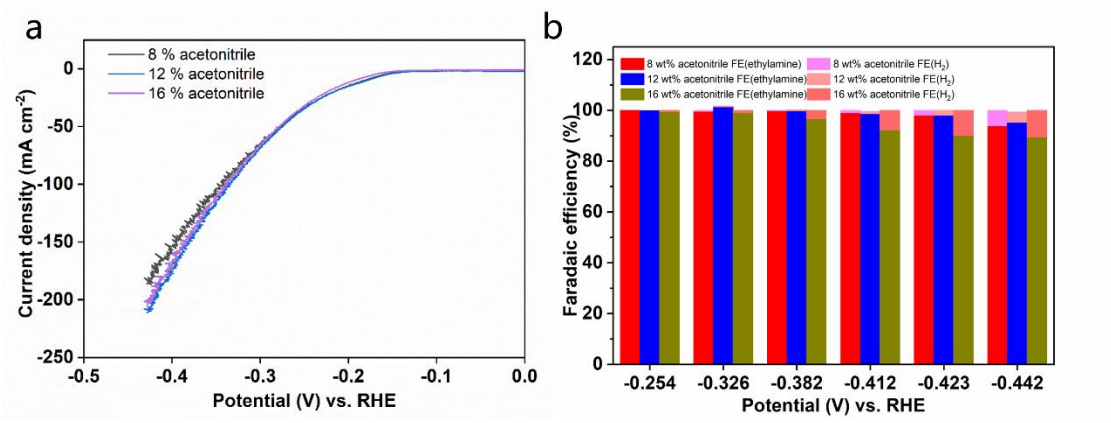

Supplementary Fig. 11 |Electrochemical measurements. (a) LSV plots of CuO@Cu in 1 M NaOH solution containing 8 wt%, 12 wt% and 16 wt% acetonitrile; (b) FE values of CuO@Cu in 1 M NaOH solution containing 8 wt%, 12 wt% and 16 wt% acetonitrile. The potentials in Supplementary Fig. 11a-b are provided after 100% iR correction. Source data for Supplementary Fig. 11 are provided as a Source Data file.

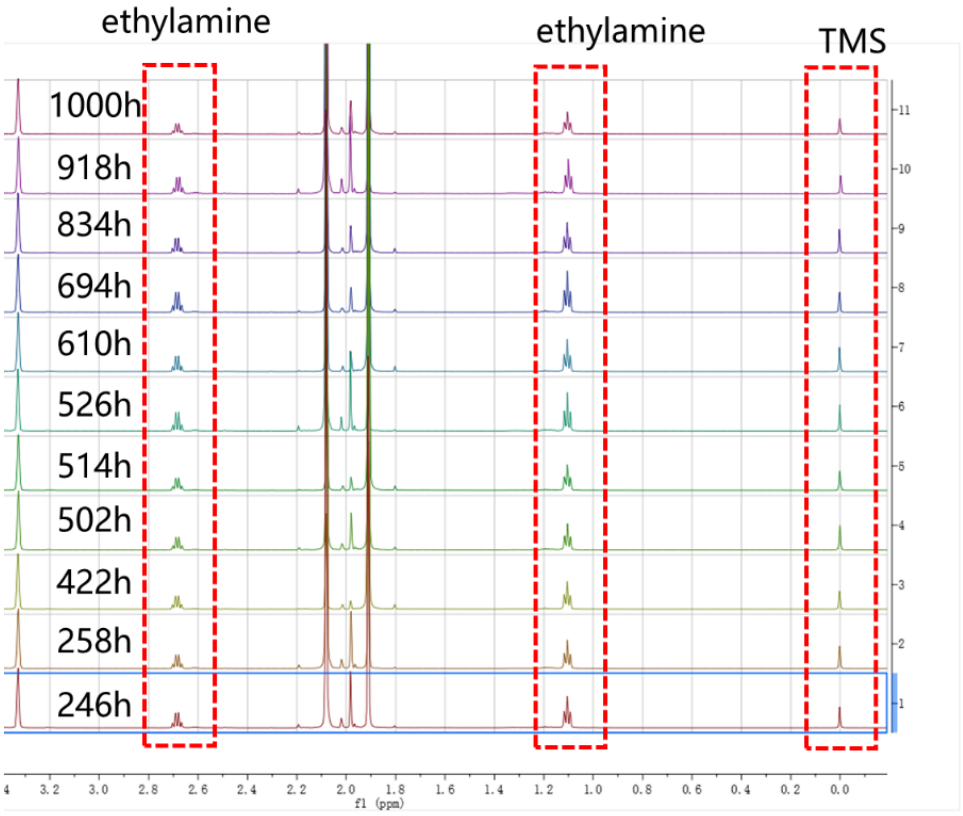

Supplementary Fig. 12 | ^{1}H NMR spectrum of the liquid products during the stability test at 200 mA cm^{-2} in a 1 M NaOH solution containing 12 wt% acetonitrile.

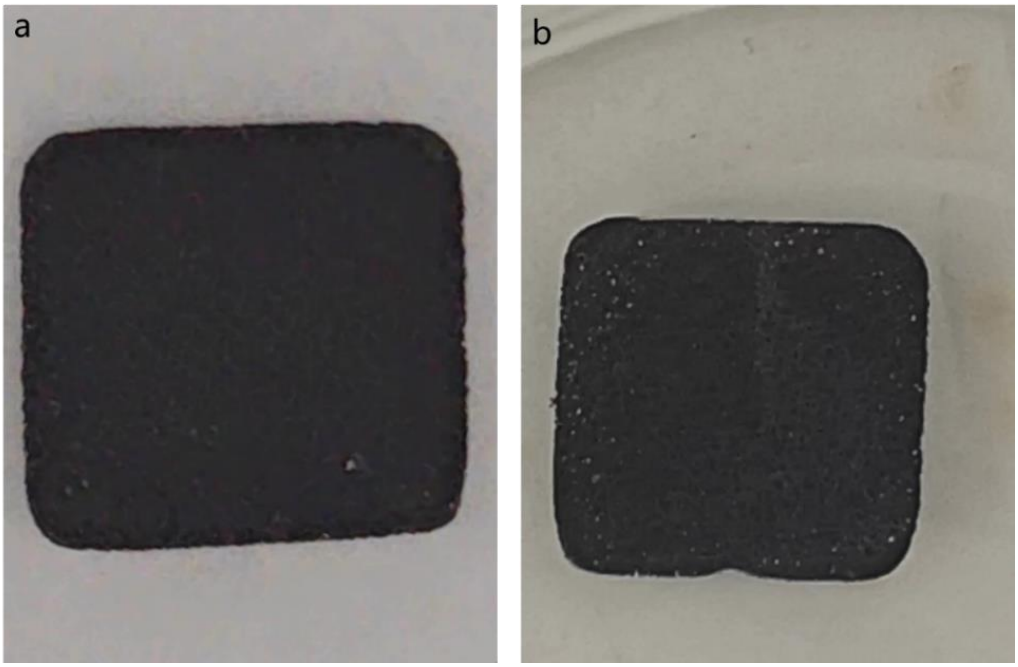

Supplementary Fig. 13 | Photos of CuO@Cu electrode. (a) initial; (b) after 1000-h stability test at a current density of 200 mA cm^{-2} in a 1 M NaOH solution containing 12 wt% acetonitrile.

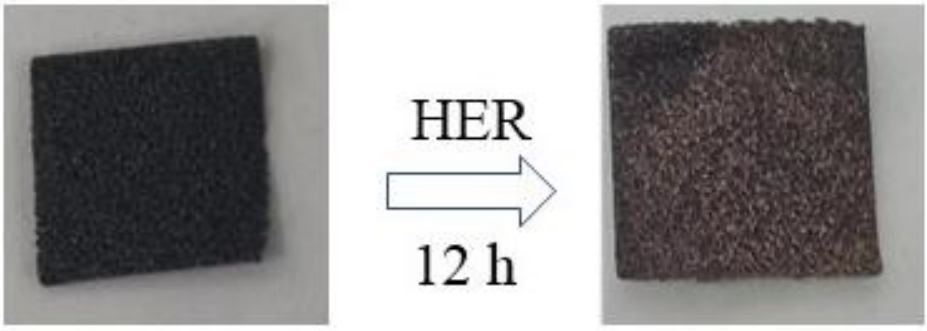

Supplementary Fig. 14 | Photos of CuO@Cu electrode before and after HER operations at a current density of 200 mA cm^{-2} in 1 M NaOH without acetonitrile.

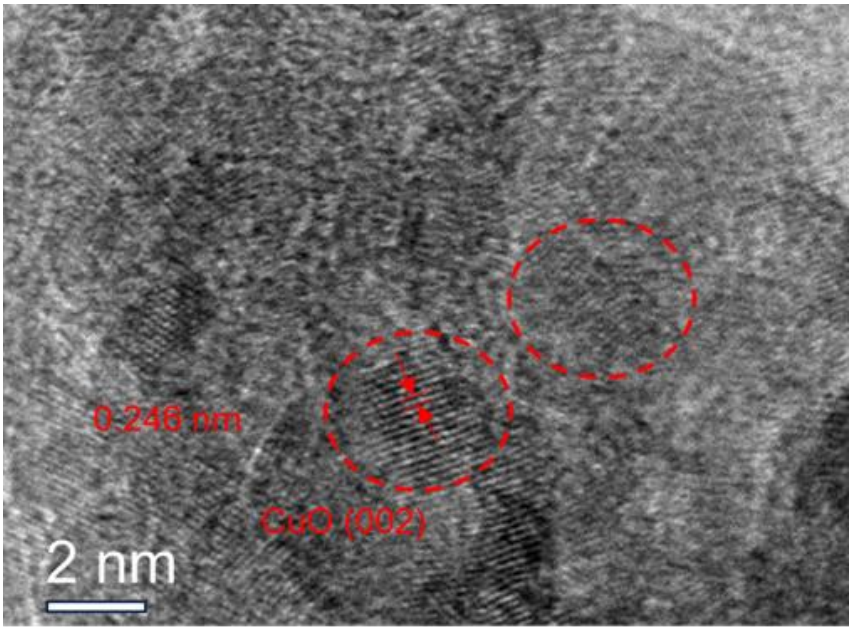

Supplementary Fig. 15 | TEM image of CuO@Cu after 1000-h stability test.

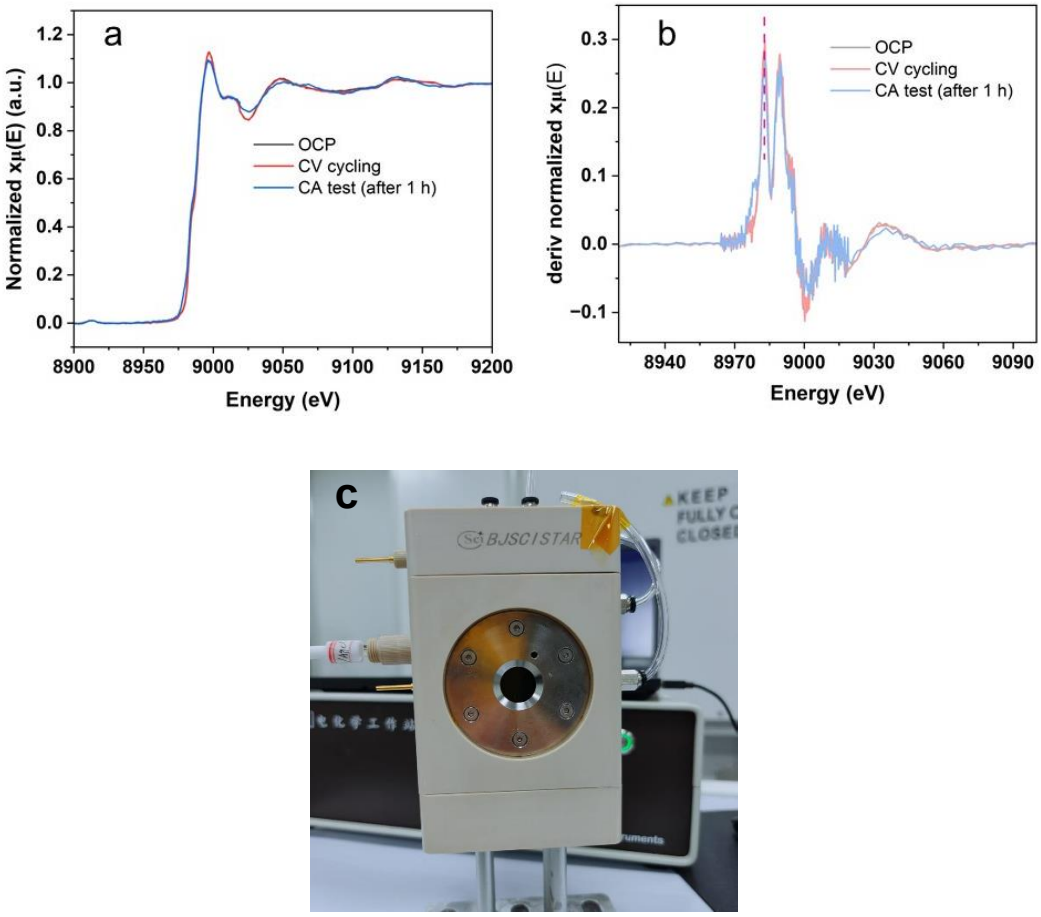

Supplementary Fig. 16 | (a) Cu K-edge XANES spectra; (b) the corresponding first derivative; (c) The photo shows the custom-built electrochemical cell designed for in-situ XAS measurements. Source data for Supplementary Fig. 16a and b are provided as a Source Data file.

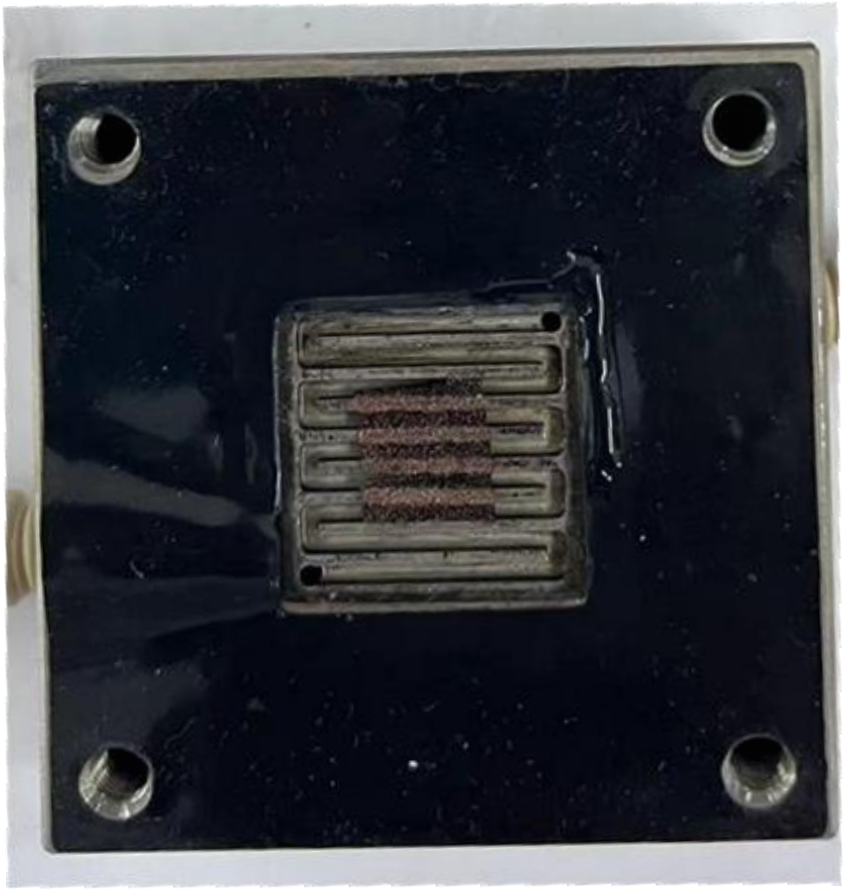

Supplementary Fig. 17 | The photo of CuO@Cu after performance test.

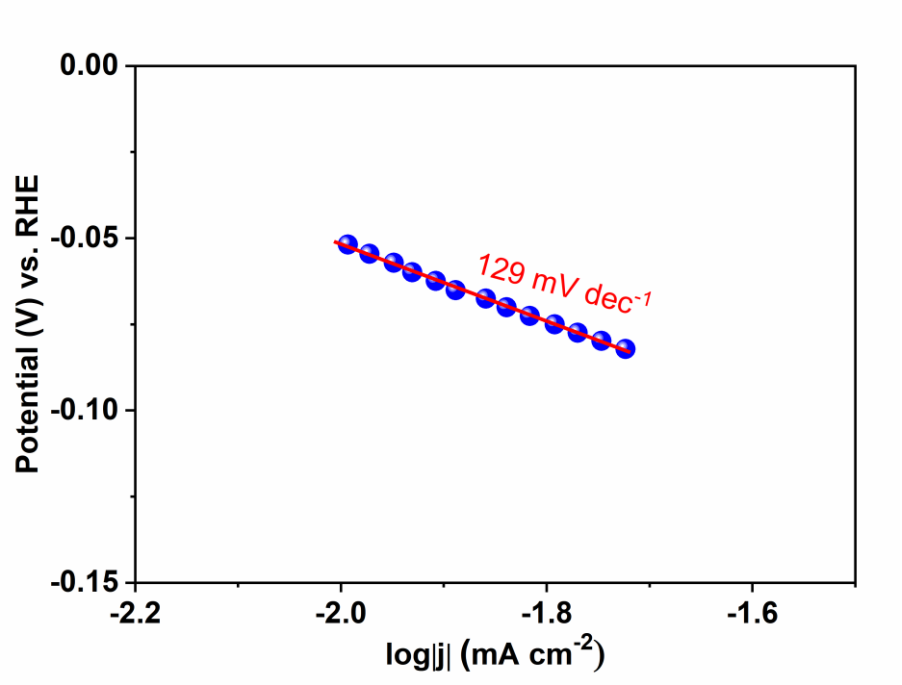

Supplementary Fig. 18 | The Tafel slope of CuO@Cu in 1 M NaOH. The potentials in Supplementary Fig. 18 are provided without iR correction. Source data for Supplementary Fig. 18 are provided as a Source Data file.

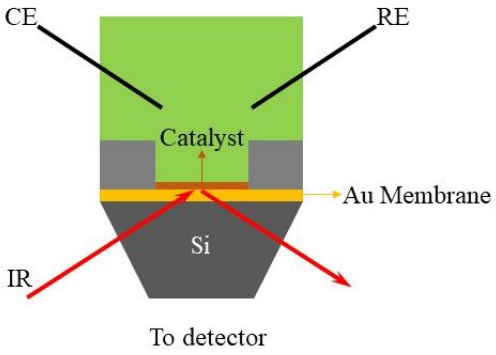

Supplementary Fig. 19 | The schematic diagram of in situ attenuated total internal reflectance Fourier transform infrared device. RE: reference electrode; CE: counter electrode.

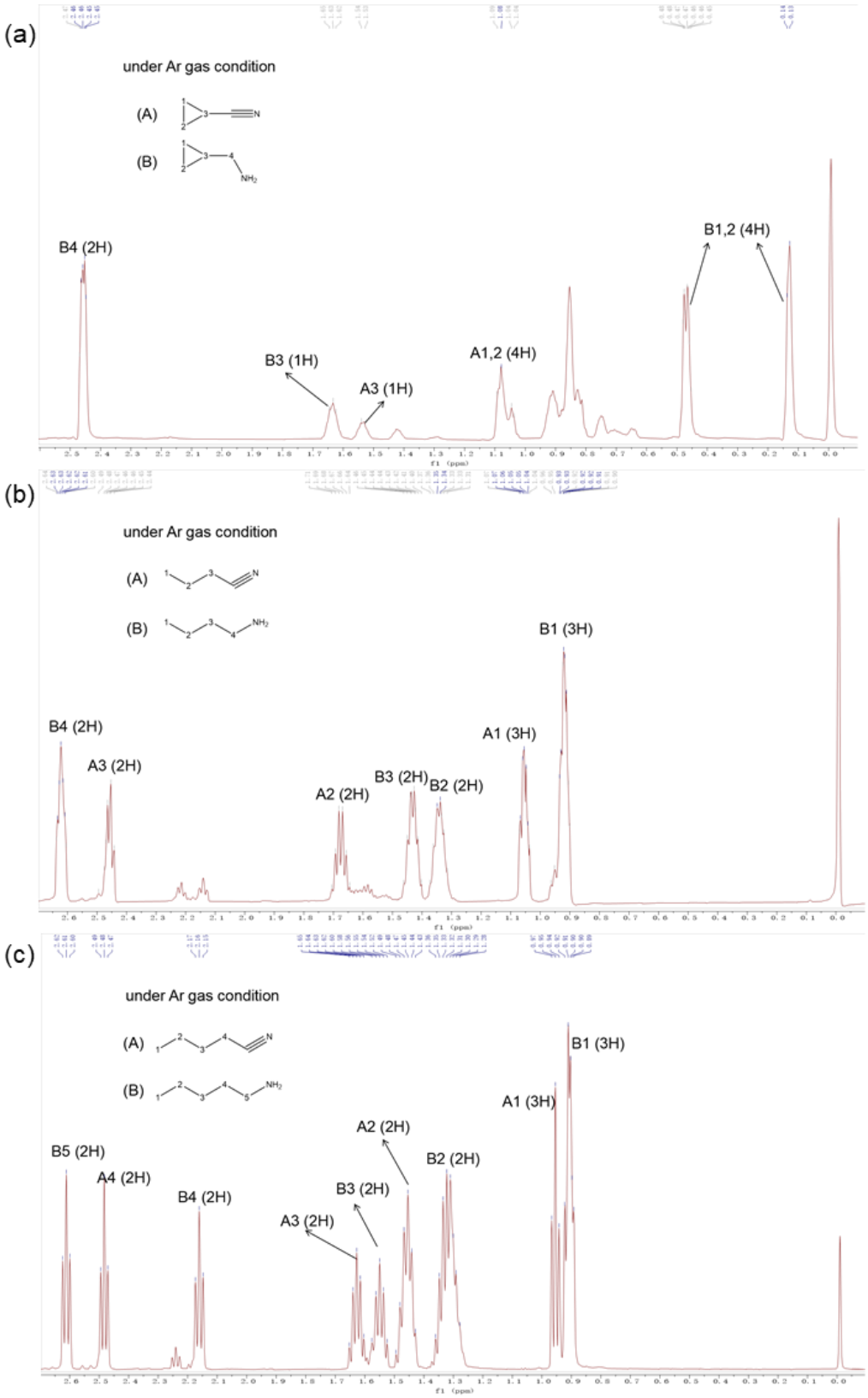

Supplementary Fig. 20 | ^{1}H NMR spectrum of the liquid products for the electrochemical hydrogenation of cyclopropanecarbonitrile (a), butyronitrile (b) and pentanenitrile (c).

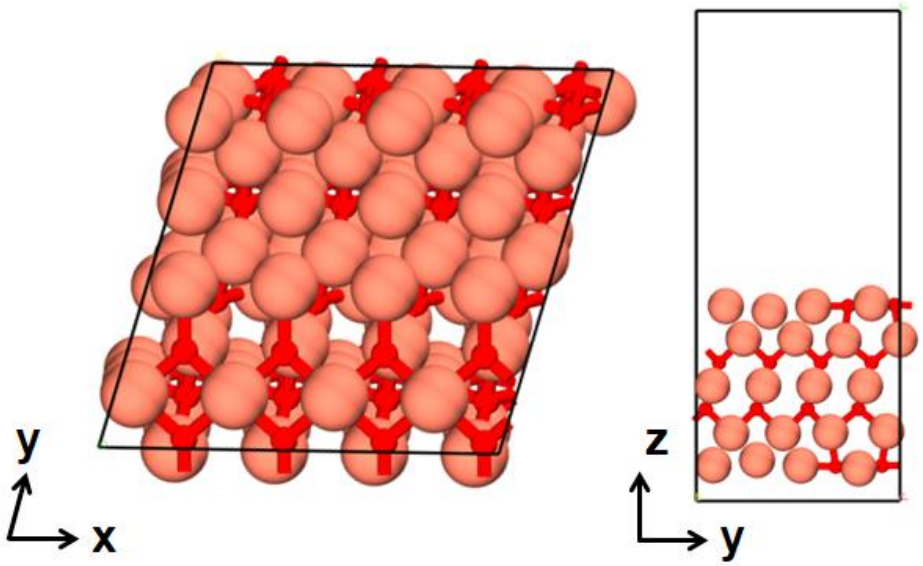

Supplementary Fig. 21 | Atomic structure of CuO_x. Top (left) and side (right) views.

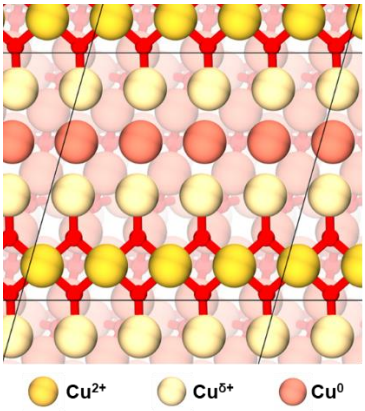

Species	Cu	Cu_2O	CuO	CuO_x surface		
Structure	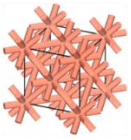	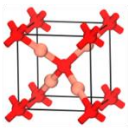	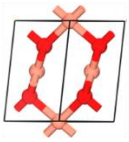			
Bader charge / |e|	0	+0.53	+0.97	+0.03	+0.24	+1.01

Supplementary Fig. 22 | Bader charge analysis of Cu in CuO_x surface, Cu, Cu_2O and CuO. The results show that the CuO_x surface comprises Cu^0, Cu^{2+} and $Cu^{\delta+}$.

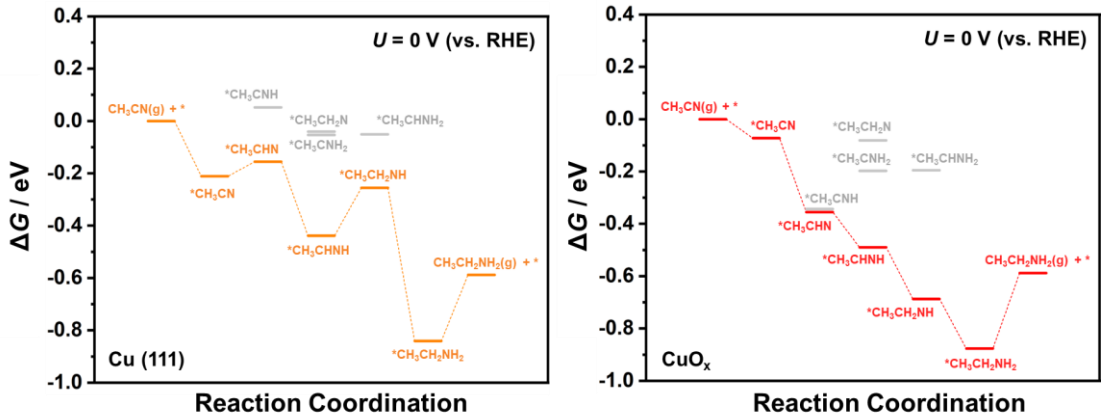

Supplementary Fig. 23 | Free energy diagrams for acetonitrile electroreduction over Cu (111) (left) and CuO_x (right) at an external potential $U = 0$ V (vs. RHE). Source data for Supplementary Fig. 23 are provided as a Source Data file.

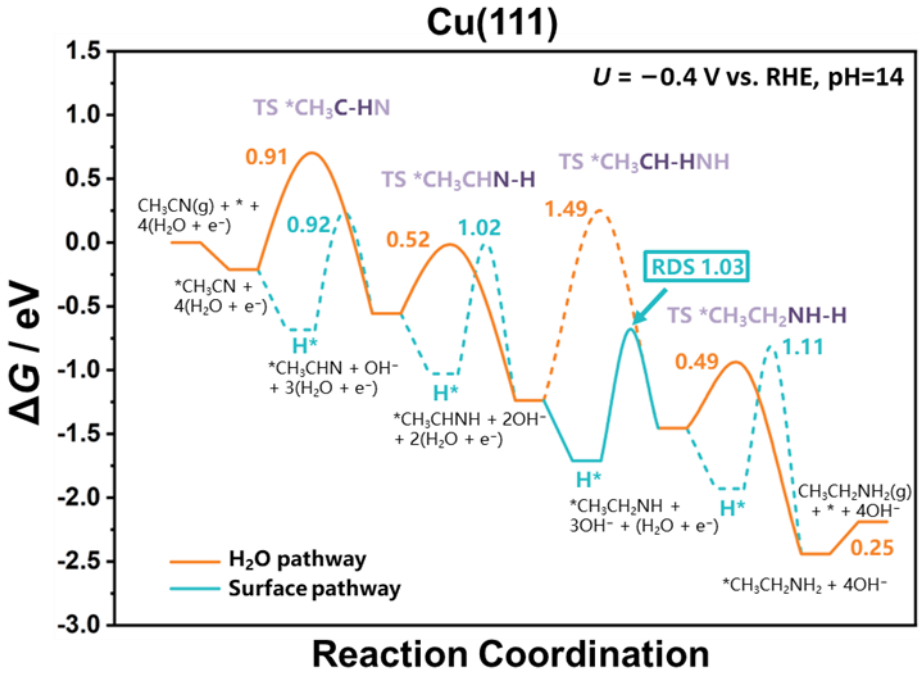

Supplementary Fig. 24 | Free energy diagrams for acetonitrile electroreduction along H_2O pathway (orange line) and surface pathway (blue line) over Cu (111) at an external potential U = −0.4 V (vs. RHE, pH = 14). Pathway with lower barrier is shown in solid line. Source data for Supplementary Fig. 24 are provided as a Source Data file.

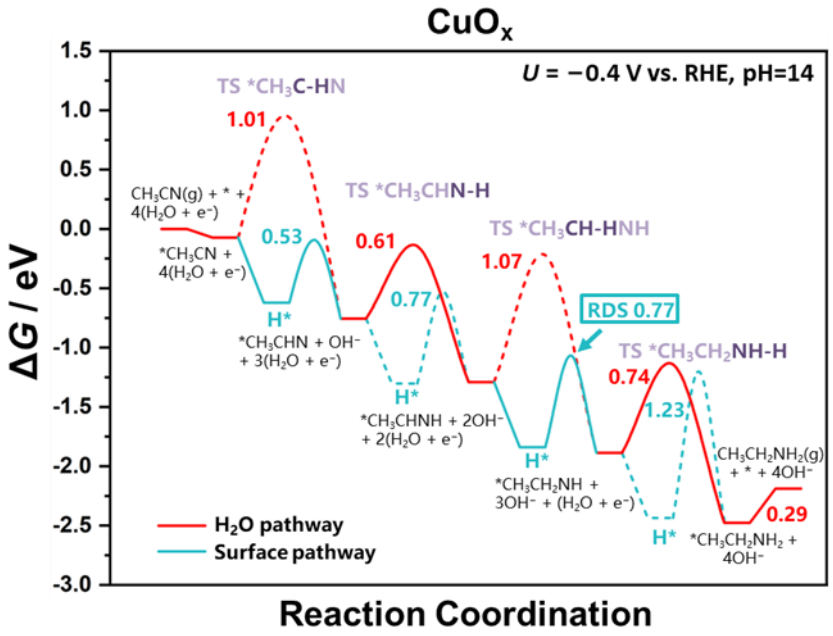

Supplementary Fig. 25 | Free energy diagrams for acetonitrile electroreduction along H_2O pathway (red line) and surface pathway (blue line) over CuO_x at an external potential U = −0.4 V (vs. RHE, pH = 14). Pathway with lower barrier is shown in solid line. Source data for Supplementary Fig. 25 are provided as a Source Data file.

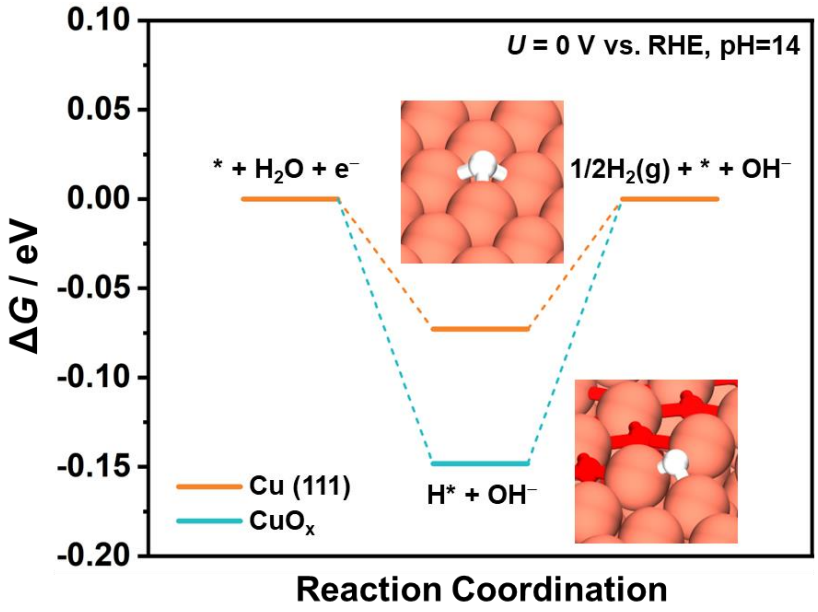

Supplementary Fig. 26 | DFT calculated free energy diagrams of HER at an applied potential U = 0 V (vs. RHE, pH = 14). Source data for Supplementary Fig. 26 are provided as a Source Data file.

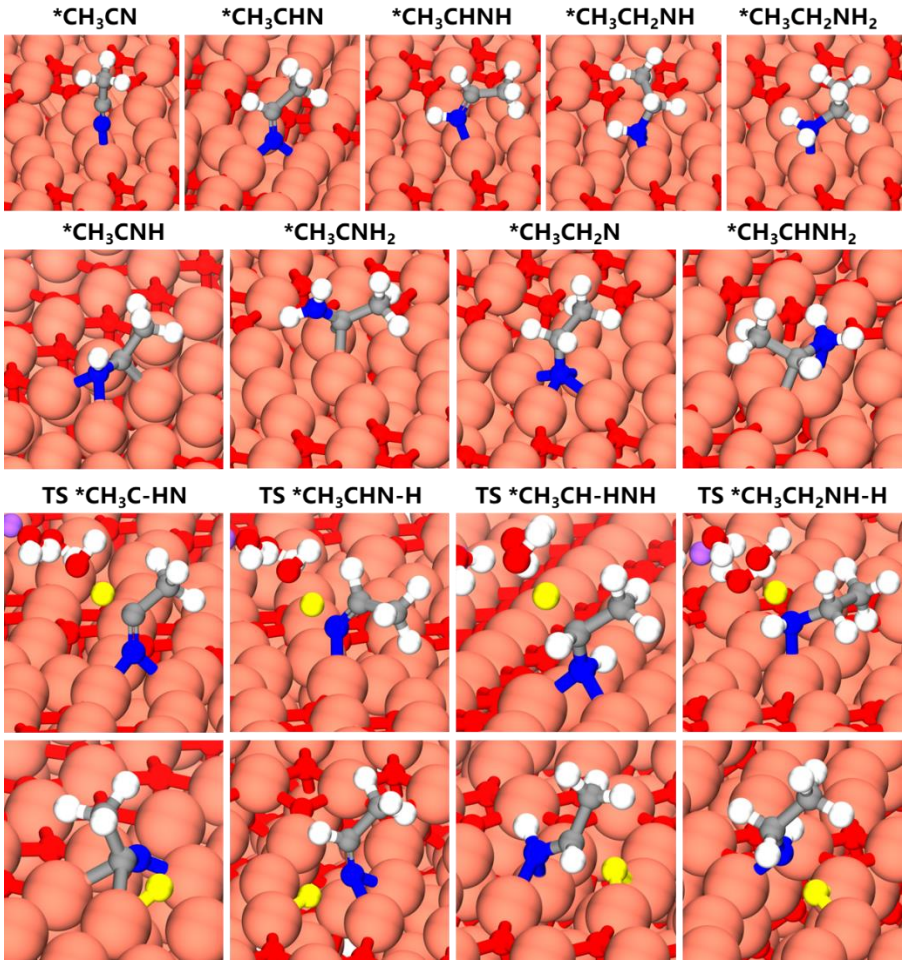

Supplementary Fig. 27 | Optimized atomic structures of reaction intermediates and transition states involved in the ARR over CuO_x. The transferred hydrogen atoms in hydrogenation steps were highlighted.

2. Supplementary Tables

Supplementary Table 1. The compensated solution resistances for different catalysts in 1M NaOH solution containing 12 wt% acetonitrile at -0.046V vs. RHE.

catalyst	$R_{\Omega 1}$	$R_{\Omega 2}$	$R_{\Omega 3}$	R_{Ω} average
CuO@Cu	1.52	1.54	1.57	1.54 ± 0.02
OD-Cu	1.31	1.29	1.31	1.30 ± 0.01
Cu-foam	1.29	1.23	1.27	1.26 ± 0.03

Supplementary Table 2. Catalysts for electroreduction of acetonitrile to ethylamine.

catalyst	electrolyte	Cell	Current density (mA cm^{-2})	Duration time (h)	Reference
CuO/Cu Foil	0.5 M $KHCO_3$ saturated with CO_2 + 0.5 M acetonitrile	H-type cell	30 (@-0.7 V vs. RHE)	2	[1]
Cu NP	1 M NaOH with 8 wt% acetonitrile	Flow cell	100	20	[2]
OD-Cu NWs	1 M NaOH with 8 wt% acetonitrile	Flow cell	400	16	[3]
Pd-Ni(OH)2	1 M KOH + 0.5 M acetonitrile	H-type cell	100 (@-0.25 V vs. RHE)	2.22	[4]
CuO@Cu	1 M NaOH with 12 wt% acetonitrile	H-type cell	200	1000	This work
CuO@Cu	1 M NaOH with 12 wt% acetonitrile	Flow cell	500	100	This work

Supplementary Table 3. Simulated vibrational modes and corresponding frequencies of various intermediates. Vibrational frequencies close to experimental ATR-FTIR results were listed. Considering the experimental frequency of C≡N stretching is 2273 cm^{-1}, a scaling factor as 0.9887 is employed to corrected the simulated frequencies,

which are labeled in the brackets.

Adsorption structures	Vibrational frequency / cm^{-1}	Vibrational mode	Experimental frequency / cm^{-1}
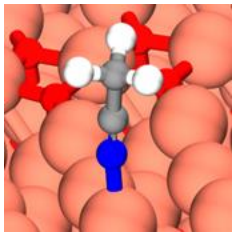	2299 (2273)	C≡N stretching	2273
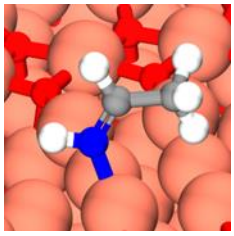	1283 (1269)	CH=NH stretching	1297
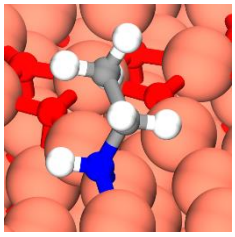	1297 (1282)	CH_2-NH stretching	
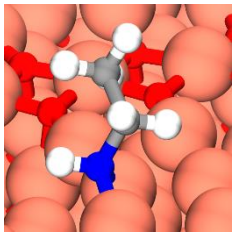	1234 (1220)	CH_3-CH_2-NH twisting	1241
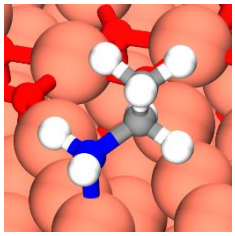	1149 (1136)	CH_2-NH_2 stretching	1133

Supplementary Table 4. Electrochemical hydrogenation of nitriles.

Entry	Nitrile	Primary amine	Selectivity (%)	FE (%)
1	cyclopropanecarbonitrile	cyclopropanemethylamine	100	81.5
2	butyronitrile	butylamine	100	66.0
3	pentanenitrile	pentylamine	100	53.6

The electrochemical hydrogen evolution reaction was performed in a 1 M NaOH aqueous solution containing nitrile (cyclopropanecarbonitrile and butyronitrile: 0.1 M, pentanenitrile: 0.2 M) in an H-type cell. The overall selectivity was evaluated by ^{1}H NMR spectroscopy, using TMS as the internal standard. The FE was evaluated based on the amount of H_2 generated, as determined by GC.

Supplementary Table 5. Bader charge (|*e*|) of hydrogen in *H, aqueous H_2O, and C, N atoms in cyano group of adsorbed acetonitrile.

	Cu (111) / |*e*|	**CuO_x / |*e*|**
***H**	−0.28	−0.23
H in H_2O	0.69	
C in -CN of *CH_3CN	0.82	0.80
N in -CN of *CH_3CN	−1.21	−1.17

3. Supplementary references

1 Zhang, D. *et al.* Highly efficient electrochemical hydrogenation of acetonitrile to ethylamine for primary amine synthesis and promising hydrogen storage. *Chem Catalysis* **1**, 393-406 (2021).

2 Xia, R. *et al.* Electrochemical reduction of acetonitrile to ethylamine. *Nat. Commun.* **12**, 1949

(2021).

3 Wei, C. *et al.* Lattice oxygen-mediated electron tuning promotes electrochemical hydrogenation of acetonitrile on copper catalysts. *Nat. Commun.* **14**, 3847 (2023).

4 Ao, W. *et al.* Electrochemical reversible reforming between ethylamine and acetonitrile on heterostructured Pd-Ni(OH)2 nanosheets. *Angew. Chem. Int. Edit.* **62** (2023).